17 O relaxation times in the rat brain at 16.4 tesla

FULL PAPER

Magnetic Resonance in Medicine 00:00–00 (2015)

^{17}O Relaxation Times in the Rat Brain at 16.4 Tesla

Hannes M. Wiesner,[1,2] Dávid Z. Balla,[1] G. Shajan,[1] Klaus Scheffler,[1,3] Kâmil Uğurbil,[2†] Wei Chen,[2] Kâmil Uludağ,[4] and Rolf Pohmann[1*†]

Purpose: Measurement of the cerebral metabolic rate of oxygen ($CMRO_2$) by means of direct imaging of the ^{17}O signal can be a valuable tool in neuroscientific research. However, knowledge of the longitudinal and transverse relaxation times of different brain tissue types is required, which is difficult to obtain because of the low sensitivity of natural abundance $H_2{}^{17}O$ measurements.
Methods: Using the improved sensitivity at a field strength of 16.4 Tesla, relaxation time measurements in the rat brain were performed in vivo and postmortem with relatively high spatial resolutions, using a chemical shift imaging sequence.
Results: In vivo relaxation times of rat brain were found to be $T_1 = 6.84 \pm 0.67$ ms and $T_2{}^* = 1.77 \pm 0.04$ ms. Postmortem $H_2{}^{17}O$ relaxometry at enriched concentrations after inhalation of $^{17}O_2$ showed similar $T_2{}^*$ values for gray matter (1.87 ± 0.04 ms) and white matter, significantly longer than muscle (1.27 ± 0.05 ms) and shorter than cerebrospinal fluid (2.30 ± 0.16 ms).
Conclusion: Relaxation times of brain $H_2{}^{17}O$ were measured for the first time in vivo in different types of tissues with high spatial resolution. Because the relaxation times of $H_2{}^{17}O$ are expected to be independent of field strength, our results should help in optimizing the acquisition parameters for experiments also at other MRI field strengths. **Magn Reson Med 000:000–000, 2015.** © **2015 Wiley Periodicals, Inc.**

Key words: relaxation times; brain water distribution; natural abundance oxygen-17; $H_2{}^{17}O$; quadrupolar relaxation; X-Nuclei; quantification; spectroscopic imaging; MRSI; ultra-high field

INTRODUCTION

In vivo imaging of oxygen metabolism, a key biological parameter for characterizing the vital status of tissue, can have a large impact in medicine and neuroscience. While most established techniques used to measure the cerebral metabolic rate of oxygen ($CMRO_2$) have the limitations of being either indirect (e.g., calibrated BOLD) (1,2) or invasive [arteriovenous difference measurements (3–5) and positron emission tomography (6)], MRI during catabolism of enriched $^{17}O_2$ to $H_2{}^{17}O$ can become a valuable alternative. However, the NMR detection of ^{17}O is challenging due to its low gyromagnetic ratio (7), short transverse relaxation times (8) and low natural abundance (9). The sensitivity of ^{17}O NMR has been shown to increase almost quadratically with field strength, supported by the field-independent relaxation times of unbound $H_2{}^{17}O$ (8,10,11). Further improvements can be realized by optimizing the acquisition parameters based on the relaxation times (12,13).

The relaxation mechanisms of the ^{17}O nucleus are significantly different from those of protons due to the spin of +5/2 (7), generally being more intramolecular as a result of quadrupolar interaction. Water as the exclusive source of the in vivo NMR signal of ^{17}O as triplet (14–16) exhibits one peak in bulk water due to fast hydrogen exchange and isotropic molecular motion (17). At physiological conditions around neutral pH, the relaxation of $H_2{}^{17}O$ is strongly influenced by chemical exchange and by temperature (15). Because field-dependent relaxation has been reported for bound water (18), a regional determination of representative relaxation times in complex in vivo tissue as a mixture of bound and free water in the brain is important for applying $CMRO_2$ imaging through $H_2{}^{17}O$ NMR detection.

In this study, we determined the regional longitudinal T_1 and apparent transverse $T_2{}^*$ relaxation times of $H_2{}^{17}O$ at natural abundance and in enriched concentrations in the rat head at 16.4T. Due to the high magnetic field and optimized measurement parameters, local differences in the relaxation times among different tissue types of rats have been observed for the first time in vivo at relatively high spatial resolutions. Additional phantom measurements were performed to assess the changes of the relaxation times with the temperature, which is critical due to the influence of viscosity and chemical exchange (19).

Previous relaxometric studies of $H_2{}^{17}O$ in rat brain have not differentiated between different tissue types in vivo. Finally, because pH, temperature, and concentrations of salts affect the chemical exchange and molecular motion, the linewidth of $H_2{}^{17}O$ is naturally autoregulated in the brain within a narrow range. Therefore, the advantages of ultra-high field MRI make it possible to obtain the necessary signal sampling efficiency at sufficient spatial resolutions and the observed field independence of the $H_2{}^{17}O$ relaxation times ensures that these results can easily be applied to studies at other field strengths.

METHODS

Instrumentation

Experiments were performed on a Bruker BioSpec Avance III system (Bruker Biospin MRI GmbH, Ettlingen,

[1]High-Field Magnetic Resonance Center, Max Planck Institute for Biological Cybernetics, Tübingen, Germany.
[2]Center for Magnetic Resonance Research, Department of Radiology, University of Minnesota Medical School, Minneapolis, Minnesota, USA.
[3]Department of Biomedical Magnetic Resonance, University of Tübingen, Tübingen, Germany.
[4]Maastricht Brain Imaging Center (M-BIC), Department of Cognitive Neuroscience, Faculty of Psychology and Neuroscience, Maastricht University, Maastricht, The Netherlands.

Grant sponsor: Max Planck Society and NIH; Grant numbers: NS41262; NS070839; P41 RR08079..

*Correspondence to: Rolf Pohmann, Ph.D., High-Field Magnetic Resonance Center, Max Planck Institute for Biological Cybernetics, Spemannstr. 41, 72076 Tübingen, Germany. E-mail: rolf.pohmann@tuebingen.mpg.de

†Drs. Uludağ and Pohmann contributed equally to this work.

Received 24 February 2015; revised 24 April 2015; accepted 21 May 2015
DOI 10.1002/mrm.25814
Published online 00 Month 2015 in Wiley Online Library (wileyonlinelibrary.com).

Germany) based on a 16.4 Tesla (T) magnet (Magnex Scientific, Abingdon, UK) with a 26-cm bore, equipped with gradients with an inner diameter of 12 cm and a maximum strength of 1 T/m within a rise time of 212 μs (Resonance Research Inc., Billerica, MA). Custom-built ^{17}O quadrature surface coils (diameter 1.5 cm; sensitive detection depth ~ 1 cm) (20) were tuned and matched for every sample individually to the ^{17}O Larmor-frequency of 94.6 MHz. The signals from 0° and 90° channels were combined by a quadrature hybrid and then amplified and digitized by a single-channel X-band receiver. Mutual coupling between the two channels, assessed by S21 measurements, was better than -20 dB. For proton imaging, a separate ^{1}H transmit and receive butterfly coil was attached on top of the ^{17}O coils.

Animal Preparation

All procedures and experiments were approved by the local authorities and carried out by FELASA qualified personnel in compliance with the guidelines of the European Community (EUVD 86/609/EEC) for the care and use of laboratory animals. A total of 14 male Wistar rats (Charles River Laboratories, Sulzfeld, Germany) were used in this study. Animals were kept at a 12/12 h day/night cycle with free access to nutrition and water.

In Vivo Measurements

Ten male Wistar rats were used for in vivo relaxometry measurements (T_1: n = 5; mean body weight 513 ± 71 g; T_2^*: n = 5; mean body weight 529 ± 30 g). Anesthesia was induced in an induction chamber by 3–4% isoflurane (Forene®, Abbott, Chicago, IL). During the preparation of the animal, anesthesia was maintained by spontaneous inhalation of room air with 2% isoflurane through an inhalation mask. A 22-gauge catheter (Venisystems Abbocath®, Abbott Laboratories, UK) was inserted into a lateral tail vein for intravenous infusion of medetomidine anesthesia. The rat head was fixated in a custom-built stereotaxic frame with the center of maximum sensitivity of the ^{17}O-coil in Z-direction close to the bregma of the rat skull. Lidocain spray (Xylocain®, AstraZeneca GmbH, Wedel, Germany) was applied topically before installation of the ear-bars. A subcutaneous bolus of Flunixin-Meglumin (5 mg/kg; Finadyne®, Essex Pharma GmbH, München, Germany) was given as analgesic for the intravenous catheter and fixation. The transition to continuous medetomidine anesthesia (Domitor®, Pfizer Inc., New York, NY) was initiated by intravenous infusion at a rate of 0.1 mg/kg/h (dilution: 0.1 mg in 1-mL saline solution with 16 IU/mL of heparin [heparin-natrium 25000®, ratiopharm GmbH, Ulm, Germany]) with successive discontinuation of isoflurane over 15–20 min (21). For the maintenance of anesthetic efficacy during long experiments (22), the medetomidine infusion rate was increased every 75 min by 50 μg/kg/h.

Breathing rate and exhaled respiration gases (Capstar-100 End-tidal CO_2 Analyzer, CWE Inc., Ardmore, PA) were monitored and recorded (PowerLab & LabChart 5; ADInstruments, Australia). Rectally measured body temperature was maintained at 36.8 ± 0.5°C by an electric heating pad connected through a radiofrequency (RF) filter. After the experiments, anesthesia was revoked using atipamezolhydrochlorid (Antisedan®, Pfizer Inc., New York, NY).

Postmortem Experiments

Four male Wistar rats (mean body weight 380 ± 131 g) were initially anesthetized with 3–4% and kept at 2% isoflurane during preparations. The animals were orally intubated for mechanical ventilation and intravenously catheterized for infusion of alpha-chloralose at 50 mg/kg/h. Rats were positioned inside the magnet and were subjected to a total approximately 90 min inhalation of 30% O_2 with a $^{17}O_2$-enrichment of 70% (Nukem GmbH, Germany) in N_2O (one rat in N_2) as part of a different study. Two hours after inhalation, the animals were killed with >5% isoflurane without changing their position within the magnet. Acquisitions started 10 min after exitus with the rat body allowed to equilibrate to ambient temperature in the magnet bore (21°C at isocenter) (23).

MRI Experiments

Adjustments

The RF-power for a nominal 90° excitation at the ^{17}O frequency was calibrated globally for each individual sample by maximizing the signal of a "pulse-and-acquire" sequence, using a 50 μs on-resonance block-pulse. For anatomical imaging and shimming, a proton surface coil was mounted on top of the ^{17}O coil assembly, while in some of the in vivo measurements a ^{1}H resonator surrounding the setup was used instead. First and second order B_0 shims were adjusted using FASTMAP (24) with a 1-ms Gaussian pulse. Proton images were acquired at high in-plane resolutions with equal slice thickness as the corresponding $H_2{}^{17}O$ images.

For in vivo $H_2{}^{17}O$ imaging, a three-dimensional (3D) chemical shift imaging (CSI) sequence using weighted averaging of the k-space was applied (25,26). To obtain sufficient signal despite the short transverse relaxation time, the acquisition delay between the middle of the excitation pulse and the start of the acquisition was minimized to 484 μs. Because a nonselective excitation pulse was used, the sensitive region in the field of view (FOV) of the 3D CSI sequence with free induction decay (FID) detection was determined by the profile of the surface coil. The raw data was Fourier transformed along the three spatial dimensions, resulting in localized FIDs, which were used to estimate T_2* times. Subsequent Fourier transformation of the time domain resulted in localized spectra. The amplitudes of the phased water peaks were used to construct the final $H_2{}^{17}O$ images.

Phantom measurements

Reference relaxation time measurements on pure water with 20 mL of a 10%-enriched $H_2{}^{17}O$ water phantom (Nukem GmbH, Germany) in a glass tube were performed at room temperature.

T_1 and T_2* were measured as described below. A region of interest (ROI) in the center of the phantom was selected to avoid potential effects of superficial heating caused by the specific absorption rate (SAR) of RF-power

and to attenuate susceptibility effects in peripheral regions of the phantom.

T_1 Relaxometry

Inversion recovery images were acquired with 20 inversion delays ranging from 0.5 ms to 45 ms in logarithmically increasing steps, using an adiabatic hyperbolic secant pulse (duration 0.5 ms, bandwidth 10 kHz) for inversion. Imaging parameters were: FOV 30 × 15.71 × 27 mm^3; matrix size 21 × 11 × 9 (nominal voxel volume 6.12 μL); relaxation delay 45 ms (TR ≫ 5 T_1); 50 μs pulse for excitation with a nominal flip angle of 90°. A total of 10,240 FIDs for each inversion step were acquired within 7–15 min (depending on the inversion time) with a maximum of 41 averages in the center of k-space. Spectroscopic data of 1250 points per FID was recorded within 10 ms with a bandwidth of 125 kHz (1321 ppm).

T_1 was determined by a mono-exponential fit of the intensity of selected voxels, using standard nonlinear least-squares algorithms (Curve Fitting Toolbox, MATLAB®, The Mathworks Inc., Natick, MA). The signal intensities for short inversion times were inverted while measurements within one standard deviation around the noise level were excluded before fitting.

The different tissue types were classified based on the proton images with reference to a rat brain atlas (27). At least two voxels between different tissue regions were not included along the outer boundary of ROIs to avoid partial volume contaminations due to the large voxel sizes in the $H_2{}^{17}O$ measurements. The T_1-measurement covered a region of 0.9 to 1.5 cm in Z-direction (depending on the size of the rat), and thus most of each rat brain. Only voxels inside the brain with a sufficient spectral signal-to-noise ratio (SNR) > 12 were fitted, which resulted in a ratio of 56% brain versus 44% muscle voxels on average.

T_2* Relaxometry In Vivo

For T_2* quantification, a short TR of 4.9 ms and a flip angle of 67.5°, close to the expected Ernst angle for the rat brain (FA = 64° for T_1 at 17.6T) (28) was used to sample 3D CSI with a FOV of 27.5 × 12.5 × 22 mm^3 and a 39 × 17 × 15 matrix (nominal voxel volume 0.76 μL). Three million FIDs (375 spectral points, bandwidth 100 kHz, 2811 averages in the center of k-space) were acquired within 4 h and 6 min from each rat.

The real part of the Fourier-transformed FID was frequency-corrected by adjusting the phase in the time-domain and fitted against a monoexponential decay. Voxel-wise estimated relaxation times were averaged over manually selected ROIs for each tissue type. Extrapolating the FIDs to zero excitation and acquisition delay resulted in T_1-weighted images, after normalizing the intensity by correcting for B_1 inhomogeneity as determined in a phantom (29).

T_2* Relaxometry Postmortem

For high-resolution anatomical images and T_2* quantification, a CSI-sequence without k-space weighting with a TR of 12 ms and a flip angle of 90° was used. To avoid RF-induced heating, the excitation pulse length was increased to 400 μs to compensate for the lack of the cooling effect of blood circulation.

A FOV of 27.5 × 12.5 × 25 mm^3 was sampled with a matrix of 41 × 19 × 25 voxels (voxel volume 0.44 μL). Approximately 2.5 million FIDs with 1000 points each and a spectral bandwidth of 100 kHz were acquired within 8 h and 18 min. Postprocessing for T_2* was then performed as in vivo.

Relaxation times are given as mean value ± standard deviation over all voxels of the selected region, with the nominal volume of the ROI added in brackets, if applicable.

Table 1
In Vivo T_1 Relaxation Times in ms of Natural Abundance $H_2{}^{17}O$ measured in the Rat Head

In vivo T_1	Muscle tissue	Brain tissue
rat 1 (583 g)	5.25 ± 1.02 (324 μL)*	6.34 ± 0.67 (477 μL)*
rat 2 (415 g)	6.47 ± 1.15 (459 μL)	6.84 ± 0.62 (441 μL)
rat 3 (483 g)	5.86 ± 1.10 (275 μL)*	7.64 ± 0.52 (282 μL)*
rat 4 (580 g)	5.22 ± 0.84 (214 μL)*	6.58 ± 0.39 (398 μL)*
rat 5 (504 g) #1	5.45 ± 0.71 (312 μL)*	6.79 ± 0.40 (398 μL)*
rat 5 (504 g) #2	5.74 ± 0.70 (312 μL)*	6.83 ± 0.45 (398 μL)*
Pop. Mean [ms]	5.67 ± 1.12*	6.84 ± 0.67*

*$P < 0.05$; significant population difference between muscle and brain tissue (paired t-test).

RESULTS

Phantom Measurements

Phantom measurements on the 10%-enriched $H_2{}^{17}O$ water sample resulted in a T_1 value of 6.24 ± 0.37 ms over the sensitive region of the surface coil, indicating stable T_1-quantification and an efficient inversion over the entire FOV. In the same phantom, a T_2* of 2.24 ± 0.09 ms was found.

In Vivo Relaxation Times T_1

T_1-values for all rats are shown in Table 1. The T_1 of brain tissue (gray and white matter) was 6.84 ± 0.67 ms and significantly higher than that of muscle (5.67 ± 1.12 ms). Muscle tissue could be clearly differentiated from brain in image intensity (Fig. 1b) and relaxation times (Fig. 1c). No significant intracerebral contrast was observed at this resolution. A repeated measurement in the same rat in a different session demonstrated highly reproducible T_1-values (Table 1; rat 5).

In Vivo and Postmortem Relaxation Times T_2*

In the high-resolution $H_2{}^{17}O$ images, intracortical structures were consistently visible due to the decreased image intensity of white matter (i.e., corpus callosum and optic radiation) against cortical gray matter in all animals, both in vivo and postmortem. T_2* of brain tissue had a mean value of 1.77 ± 0.04 ms and did not vary significantly between white and gray matter (Fig. 2c; Table 2a), while being significantly increased in cerebrospinal fluid (CSF), e.g., in the ventricles (in vivo: 2.21 ± 0.20 ms; postmortem: 2.30 ± 0.16 ms, Table 2). A $T_2{}^*$ of ~4 ms was measured in the eyes, too small in volume for quantitative evaluation. No significant deviation from a single exponential relaxation behavior was

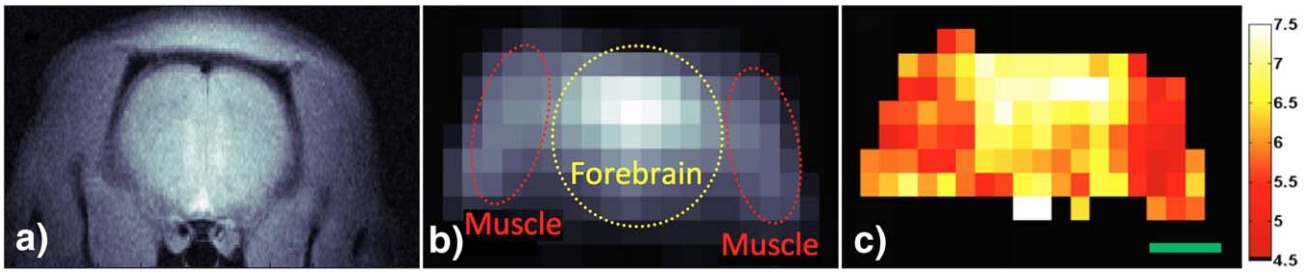

FIG. 1. Longitudinal relaxation time T_1. **a:** Proton FLASH image of a coronal slice in the rat head in vivo. **b:** Signal intensity of the $H_2{}^{17}O$ spectral peak at natural abundance concentration of the same slice with delineations of forebrain (yellow) and surrounding muscle (red). **c:** Corresponding slice of $H_2{}^{17}O$ in vivo T_1 relaxation times with clear differences between brain and muscle tissue. A 5-mm scale bar (green) is shown for the colocalized slices.

apparent in the signal time course of the localized FIDs as used for the T_2* estimations (Fig. 3a). Extrapolation to TE = 0 yielded combined spin density- and T_1-weighted images (Fig. 3c), showing highest signal intensity in muscle tissue and lowest in CSF and ventricles, confirming the lower T_1 in muscle than in brain (Fig. 1c).

Rats undergoing $^{17}O_2$-inhalations which were used for the postmortem T_2* measurements showed a global increase of the image intensity by a factor of 4 to 5 compared with the natural abundance $H_2{}^{17}O$ signal, due to significant metabolic conversion of $^{17}O_2$ to $H_2{}^{17}O$. No intracortical difference from metabolic rates (e.g., between white and gray matter) was detectable, due to the long duration of anatomical acquisition (i.e., diffusion of locally elevated $H_2{}^{17}O$ concentration in equilibrium due to exhaustion of concentration gradients). Postmortem T_2* values in muscle, GM and WM tissue were slightly increased compared with in vivo data, whereas the difference between brain tissue and CSF remained similar (Table 2b). This was accompanied by a generally decreased image contrast in the postmortem measurements, especially in regions with high water content (Fig. 4).

DISCUSSION

In this study, we have taken advantage of the increased signal at ultra-high magnetic field to quantify $H_2{}^{17}O$ relaxation times in the rat brain in vivo, for the first time differentiating different tissue types with relatively high spatial resolution. The results of this study should be beneficial to design future experiments, but also to assess the results of previous quantitative examinations. While a spectroscopic technique was used in all acquisitions to reach high sensitivity for the rats with and without $^{17}O_2$ inhalation, no metabolite peaks except the water signal were observable in our spectra (30–34) because of the limited excitation bandwidth in relation to the large range of chemical shifts with molecules containing ^{17}O.

Phantom Studies

Our phantom measurements are in relative agreement with results from previous nonlocalized measurements which reported values of T_1 around 6–8 ms for enriched pure water (35) at physiological temperatures. Temperature controlled T_2* measurements using continuous wave NMR reported T_2* up to 4 ms at enriched $H_2{}^{17}O$ concentrations (36,37) in contrast to our significantly lower values, which could be a result of the higher achievable B_0 field-homogeneity in nonlocalized NMR spectroscopy, of better temperature control in the nonlocalized measurements in NMR spectrometers and higher purity from paramagnetic ions of the glassware being

Table 2
In Vivo and Postmortem T_2^* Relaxation Times in ms of $H_2{}^{17}O$ measured in the Rat Head

a) In vivo T_2^* (natural abundance)				
	Muscle tissue	WM	GM	CSF
rat A (567 g)	1.03 ± 0.18 (309 μL)	1.86 ± 0.15 (24 μL)	1.83 ± 0.13 (111 μL)	2.56 ± 0.23 (38 μL)
rat B (499 g)	1.07 ± 0.18 (296 μL)	1.78 ± 0.09 (29 μL)	1.75 ± 0.08 (126 μL)	2.19 ± 0.12 (27 μL)
rat C (503 g)	1.08 ± 0.17 (301 μL)	1.75 ± 0.11 (25 μL)	1.73 ± 0.10 (128 μL)	2.13 ± 0.16 (28 μL)
rat D (526 g)	1.15 ± 0.16 (361 μL)	1.71 ± 0.10 (20 μL)	1.77 ± 0.08 (148 μL)	2.14 ± 0.11 (27 μL)
rat E (552 g)	1.27 ± 0.15 (315 μL)	1.77 ± 0.08 (14 μL)	1.76 ± 0.15 (100 μL)	2.05 ± 0.11 (10 μL)
Pop. Mean [ms]	1.12 ± 0.09*	1.77 ± 0.06	1.77 ± 0.04	2.21 ± 0.20*
b) Postmortem T_2^* (enriched ~4–5 times of natural abundance)				
rat F (250 g)	1.30 ± 0.21 (232 μL)	1.81 ± 0.17 (33 μL)	1.83 ± 0.15 (199 μL)	2.27 ± 0.35 (14 μL)
rat G (430 g)	1.28 ± 0.16 (239 μL)	1.84 ± 0.21 (25 μL)	1.85 ± 0.17 (182 μL)	2.26 ± 0.39 (9 μL)
rat H (540 g)	1.29 ± 0.25 (276 μL)	1.91 ± 0.33 (24 μL)	1.92 ± 0.21 (102 μL)	2.14 ± 0.44 (8 μL)
rat I (300 g)	1.20 ± 0.16 (207 μL)	1.87 ± 0.16 (22 μL)	1.89 ± 0.12 (175 μL)	2.53 ± 0.35 (25 μL)
Pop. Mean [ms]	1.27 ± 0.05*	1.86 ± 0.04	1.87 ± 0.04	2.30 ± 0.16*

*$P < 0.01$ significant population difference between muscle/CSF and brain tissue (paired t-test).

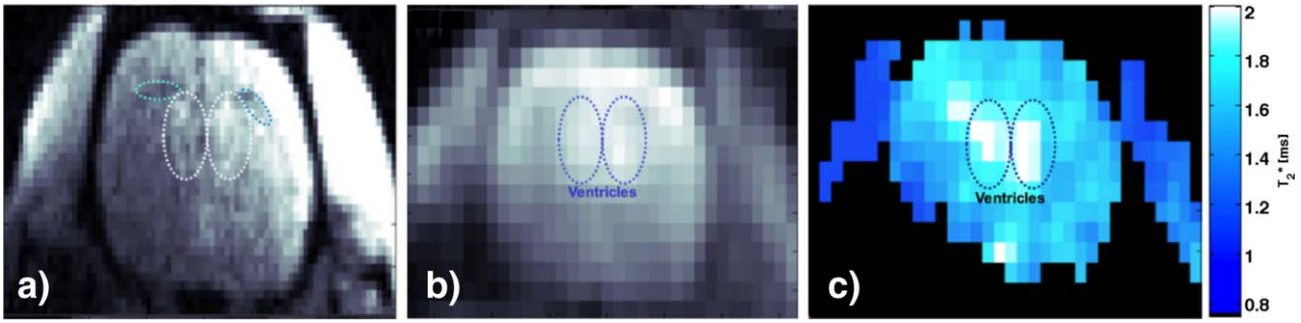

FIG. 2. Apparent in vivo transverse relaxation time T_2^*. **a:** Coronal FLASH proton image. **b:** CSI anatomical contrast of rat tissues in image intensity of $H_2{}^{17}O$ with intra-cortical differentiations of white matter and ventricles. **c:** T_2^* estimates of $H_2{}^{17}O$ with pronounced differentiation between brain parenchyma (gray matter, white matter) and cerebrospinal fluid in the ventricles.

used (35). Furthermore, a fair amount of one-dimensional experiments in the 1970s accumulated in vitro estimations of muscle tissue T_1 and T_2 (37–39). In contrast to proton MRI, T_2^* contrast changes close to air-sample borders were not observed in any images nor with varying voxel sizes as the frequency of $H_2{}^{17}O$ at

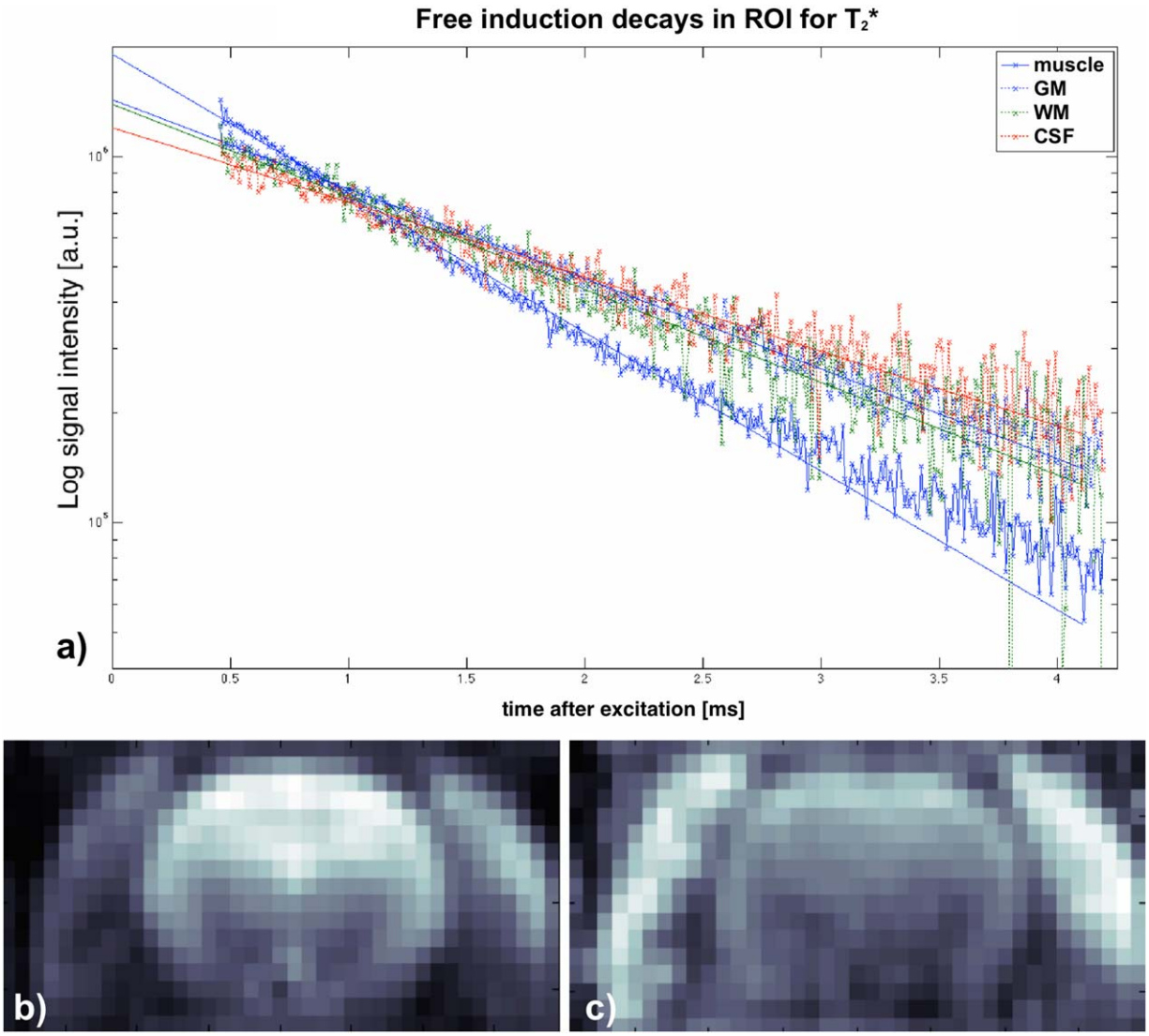

FIG. 3. **a:** Semi-logarithmic plot of the MR-signal (real part) averaged over ROIs of one rat from the in vivo measurements with fitted T_2^* relaxation curves for four tissue types. Free induction decays of different tissue types show high linearity without pronounced modulations. **b:** Reconstructed image of muscle and brain tissue based on the spectral peak of $H_2{}^{17}O$. **c:** T_1-weighted image generated by extrapolation of the FIDs (see text) to an acquisition delay of $t = 0$ for the same coronal slice as shown in b).

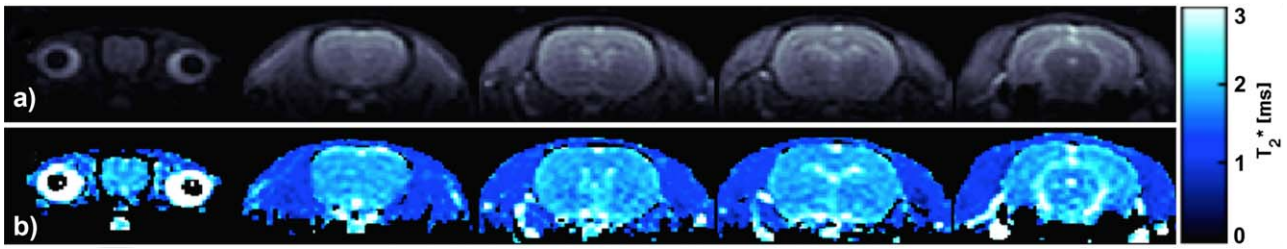

FIG. 4. Apparent postmortem transverse relaxation time T_2^*. **a:** Postmortem images with increased $H_2{}^{17}O$ concentration due to metabolic enrichment after inhalation of $^{17}O_2$ gas. Olfactory bulb, forebrain, thalamus and cortex are shown with clear contrast between white matter (corpus callosum) and ventricles. **b:** T_2^* map of the same slices as in a) exhibiting slightly increased relaxation times in cortical fluids of the ventricles.

16.4 Tesla used in this study translates to a larmor frequency of 2.2T for protons. In addition, peak intensity changed by less than 15% comparing unlocalized spectra with and without B_0-shimming, (i.e., with a smaller change in T_2^*).

Tissue Specific Relaxation and Anatomical Contrast

The differences between muscle and brain tissue $H_2{}^{17}O$ relaxation times have similar proportions as those known from proton measurements (40–42) and cannot be explained from temperature difference alone. However, intracortical differences are much less pronounced than for proton MRI due to the limited influence of the intermolecular environment on the field-independent relaxation of $H_2{}^{17}O$ (43). The lack of differentiable T_2^* relaxation times between gray and white matter and the clear separation by low intensity of white matter structures indicate a difference in either T_1 or in $H_2{}^{17}O$ concentration (Fig. 3c). The latter could be due to the variations in water content of more than 15% between gray and white matter as found in the human brain (44) and could affect natural abundance $H_2{}^{17}O$ calibration (45).

The higher intersubject variability of the T_1 measurements compared with the T_2^* data (Table 1 versus 2) is mainly due the lower sensitivity of the inversion recovery sequence compared with the simple FID acquisition used to determine T_2^*. In part, choosing larger voxels for the T_1 measurements compensated for this. However, the low sensitivity of $H_2{}^{17}O$ in general requires multiple repetitions for averaging the signal both in T_1 and T_2^* measurements, which is possible due to the generally short T_1 in contrast to more slowly relaxing nuclei like protons.

Most previous investigations on oxygen consumption were limited in localization because of the low sensitivity of the ^{17}O nucleus, thus neglecting potential contributions from nonbrain tissue. In animal studies using surface coils for detection, the signal from muscles could cause significant confound, owing to the property of small coils to overemphasize superficial (i.e., proximal) anatomical structures. However, our results indicate that the low T_2^* values in muscle tissues presented here assure that the signal contribution from this tissue type will play a less dominating role when sufficiently long TE is used.

While the still relatively large voxels sizes may lead to residual partial volume effects, further increasing the spatial resolution, which is constricted by the low SNR of the measurements, will be challenging. In our experiments, we have chosen a CSI sequence because of its high SNR efficiency and its short acquisition delay. The necessary SNR gain for improving the resolution might be possible by further reducing the signal loss due to transverse relaxation by using imaging sequences with ultrashort or even zero TE.

Comparison of In Vivo and Postmortem

Differences between in vivo and postmortem relaxation times reflect well known effects from previous studies (e.g., due to cell rupture, increased diffusion between intra- and extracellular space and differences in temperature) (23,46). Temperature changes due to the rapid succession of RF-pulses can distort the resulting relaxation times especially in the postmortem measurements, where the body temperature is lower and no perfusion dissipates the heat. While SAR was reduced in these measurements by increasing the pulse duration, regions close to the coil, especially in the skeletal muscles, may heat up, explaining the slightly higher T_2^* in those regions. In the ex vivo measurements, it was possible to reach

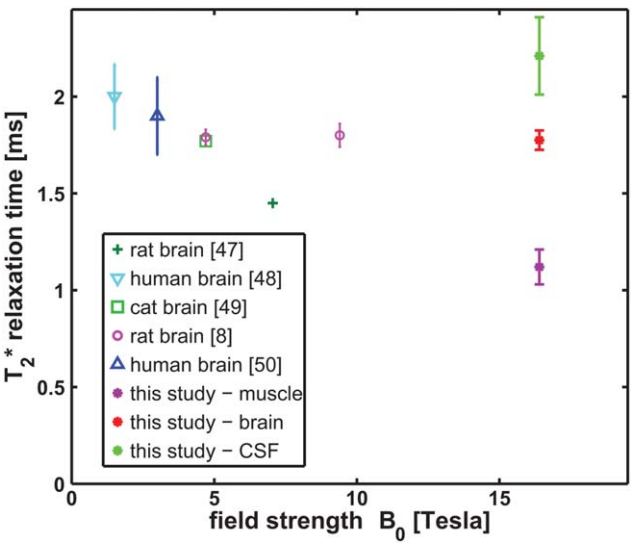

FIG. 5. Literature comparison of T_2^* relaxation times at different B_0 field strength of in vivo brain tissue. Span of error bar equals standard deviation, if available.

even higher spatial resolutions due to the $H_2{}^{17}O$ enrichment and the long measurement times.

^{17}O Relaxation Times across Field Strength

In contrast to proton MRI, the longitudinal and transverse relaxation times of $H_2{}^{17}O$ are expected to be independent of field strength. Figure 5 shows an overview of previously published T_2*-values at different field strengths (8,47–50), including the results from the current study. All brain tissue T_2* values are remarkably close around 1.8 ms, because the tissue is maintained in an autoregulatory regime of temperature and pH, some of the most dominant factors for transverse $H_2{}^{17}O$ relaxation. This data is consistent with the assumption of field-independent relaxation times, albeit a slight tendency to shorter T_2* (Fig. 5) might be visible in muscle tissue.

Differences to previous studies might be due to differences in temperature, which may result from convection effects or the different temperature controlling procedures. They can also be caused by RF-heating in in vivo experiments, because the short T_1 and T_2* and the necessity of rapid averaging increase SAR. For ^{17}O experiments at high fields, SAR monitoring and reduction is critical especially with humans. Thus, in the postmortem study we used longer RF excitation pulses to avoid excessive heating at the expense of signal loss due to relaxation during the pulse. Further discrepancies between the current study and previous experiments may be due to differences in the sampled tissue, because most previous in vivo data were acquired with limited spatial localization and might represent a different mixture of tissue types.

CONCLUSIONS

The use of ultrahigh field strength made it possible to determine tissue specific ^{17}O relaxation parameters. These might be used for sequence optimization (13,51) and analysis of data acquired using short TR during inhalation of enriched $^{17}O_2$ gas for the determination of $CMRO_2$. Due to the apparent field independence of the ^{17}O relaxation times, the results can easily be transferred to lower field strengths, as long as tissue and temperature differences are taken into account.

ACKNOWLEDGMENTS

We thank Hellmut Merkle and Michael Beyerlein for advice on RF-coils and animal setup. The study was funded by the Max Planck Society and supported in part by NIH grants.

REFERENCES

1. Davis TL, Kwong KK, Weisskoff RM, Rosen BR. Calibrated functional MRI: mapping the dynamics of oxidative metabolism. Proc Natl Acad Sci U S A 1998;95:1834–1839.
2. Hoge RD, Atkinson J, Gill B, Crelier GR, Marrett S, Pike GB. Linear coupling between cerebral blood flow and oxygen consumption in activated human cortex. Proc Natl Acad Sci U S A 1999;96:9403–9408.
3. Gotoh F, Meyer JS, Takagi Y. Cerebral effects of hyperventilation in man. Arch Neurol 1965;12:410–423.
4. Gotoh F, Meyer JS, Ebihara S. Continuous recording of human cerebral blood flow and metabolism: methods for electronic monitoring of arterial and venous gases and electrolytes. Med Res Eng 1966;5:13–19.
5. Meyer JS, Gotoh F, Favale E. Cerebral metabolism during epileptic seizures in man. Electroencephalogr Clin Neurophysiol 1966;21:10–22.
6. Mintun MA, Raichle ME, Martin WRW, Herscovitch P. Brain oxygen utilization measured with O-15 radiotracers and positron emission tomography. J Nucl Med 1984;25:177–187.
7. Alder F, Yu FC. On the spin and magnetic moment of 17O. Phys Rev 1951;81:1067–1068.
8. Zhu X-H, Merkle H, Kwag J-H, Ugurbil K, Chen W. 17O relaxation time and NMR sensitivity of cerebral water and their field dependence. Magn Reson Med 2001;45:543–549.
9. Berglund M, Wieser ME. Isotopic compositions of the elements 2009 (IUPAC Technical Report). Pure Appl Chem 2011;83:397–410.
10. Thelwall PE, Blackband SJ, Chen W. Field dependence of 17O T1, T2 and SNR - in vitro and in vivo studies at 4.7, 11 and 17.6 Tesla. In Proceedings of the 11th Annual Meeting of ISMRM, Toronto, ON, Canada; 2003. p. 504.
11. Lu M, Zhang Y, Ugurbil K, Chen W, Zhu X-H. In vitro and in vivo studies of 17O NMR sensitivity at 9.4 and 16.4 T. Magn Reson Med 2013;69:1523–1527.
12. Becker ED, Ferretti JA, Gambhir PN. Selection of optimum parameters for pulse Fourier transform nuclear magnetic resonance. Anal Chem 1979;51:1413–1420.
13. Pohmann R, von Kienlin M, Haase A. Theoretical evaluation and comparison of fast chemical shift imaging methods. J Magn Reson 1997;129:145–160.
14. Meiboom S. Nuclear magnetic resonance study of the proton transfer in water. J Chem Phys 1961;34:375–388.
15. Hertz HG, Klute R. The slowing down of proton exchange in aqueous solutions of structure breaking ions. Z Phys Chem (N F) 1970;69:101–107.
16. Okroyan G, Kushnarev D, Kalabin G, Proidakov A. Spin–spin relaxation in the 17O NMR spectra of Na+ and K+ water clusters. J Struct Chem 2002;43:242–245.
17. Redfield AG. On the theory of relaxation processes. IBM J Res Dev 1957;1:19–31.
18. Denisov VP, Halle B. Thermal denaturation of ribonuclease A characterized by water 17O and 2H magnetic relaxation dispersion. Biochemistry 1998;37:9595–9604.
19. Boykin DW. 17O NMR spectroscopy in organic chemistry. London: CRC press; 1991.
20. Kumar A, Bottomley P. Optimized quadrature surface coil designs. Magn Reson Mater Phy 2008;21:41–52.
21. Weber R, Ramos-Cabrer P, Wiedermann D, van Camp N, Hoehn M. A fully noninvasive and robust experimental protocol for longitudinal fMRI studies in the rat. Neuroimage 2006;29:1303–1310.
22. Pawela CP, Biswal BB, Hudetz AG, Schulte ML, Li R, Jones SR, Cho YR, Matloub HS, Hyde JS. A protocol for use of medetomidine anesthesia in rats for extended studies using task-induced BOLD contrast and resting-state functional connectivity. Neuroimage 2009;46:1137–1147.
23. Fagan AJ, Mullin JM, Gallagher L, Hadley DM, Macrae IM, Condon B. Serial postmortem relaxometry in the normal rat brain and following stroke. J Magn Reson Imaging 2008;27:469–475.
24. Gruetter R. Automatic, localized in vivo adjustment of all first- and second-order shim coils. Magn Reson Med 1993;29:804–811.
25. Brown TR, Kincaid BM, Ugurbil K. NMR chemical shift imaging in three dimensions. Proc Natl Acad Sci U S A 1982;79:3523–3526.
26. Pohmann R, von Kienlin M. Accurate phosphorus metabolite images of the human heart by 3D acquisition-weighted CSI. Magn Reson Med 2001;45:817–826.
27. Paxinos G, Watson C. The rat brain in stereotaxic coordinates, 6th edition. Boston: Academic Press; 2006.
28. Thelwall PE. Detection of 17O-tagged phosphate by 31P MRS: a method with potential for in vivo studies of phosphorus metabolism. Magn Reson Med 2007;57:1168–1172.
29. Axel L, Costantini J, Listerud J. Intensity correction in surface-coil MR imaging. AJR Am J Roentgenol 1987;148:418–420.
30. Irving CS, Lapidot A. Haemoglobin-17O2 revisited. Nat New Biol 1971;230:224.
31. Oldfield E, Lee HC, Coretsopoulos C, Adebodun F, Park KD, Yang S, Chung J, Phillips B. Solid-state oxygen-17 nuclear magnetic resonance spectroscopic studies of 17O2 picket fence porphyrin, myoglobin, and hemoglobin. J Am Chem Soc 1991;113:8680–8685.

32. Lee HC, Oldfield E. Oxygen-17 nuclear magnetic resonance-spectroscopic studies of carbonmonoxy hemoproteins. J Am Chem Soc 1989;111:1584–1590.
33. Gerothanassis IP. 17O NMR studies of hemoproteins and synthetic model compounds in the solution and solid states. Prog Nucl Magn Reson Spectrosc 1994;26(Pt 3):239–292.
34. De Graaf RA, Brown PB, Rothman DL, Behar KL. Natural abundance 17O NMR spectroscopy of rat brain in vivo. J Magn Reson 2008;193: 63–67.
35. Hindman JC, Svirmickas A, Wood M. Spin-lattice relaxation of oxygen-17 in water. J Phys Chem 1970;74:1266–1269.
36. Garrett BB, Denison AB, Rabideau SW. Oxygen-17 relaxation in water. J Phys Chem 1967;71:2606–2611.
37. Swift TJ, Barr EM. An oxygen magnetic resonance study of water in frog skeletal muscle. Ann N Y Acad Sci 1973;204:191–196.
38. Civan MM, Shporer M. 17O Nuclear magnetic resonance spectrum of H217O in frog striated muscle. Biophys J 1972;12:404–413.
39. Fung BM, McGaughy TW. Study of spin-lattice and spin-spin relaxation times of 1H, 2H, and 17O in muscular water. Biophys J 1979;28: 293–303.
40. Crémillieux Y, Ding S, Dunn JF. High-resolution in vivo measurements of transverse relaxation times in rats at 7 Tesla. Magn Reson Med 1998;39:285–290.
41. Stanisz GJ, Odrobina EE, Pun J, Escaravage M, Graham SJ, Bronskill MJ, Henkelman RM. T1, T2 relaxation and magnetization transfer in tissue at 3T. Magn Reson Med 2005;54:507–512.
42. Pohmann R, Shajan G, Balla DZ. Contrast at high field: relaxation times, magnetization transfer and phase in the rat brain at 16.4 T. Magn Reson Med 2011;66:1572–1581.
43. Glasel JA. A study of water in biological systems by O17 magnetic resonance spectroscopy. II. Relaxation phenomena in pure water. Proc Natl Acad Sci U S A 1967;58:27–33.
44. Whittall KP, Mackay AL, Graeb DA, Nugent RA, Li DKB, Paty DW. In vivo measurement of T2 distributions and water contents in normal human brain. Magn Reson Med 1997;37:34–43.
45. Atkinson IC, Thulborn KR. Feasibility of mapping the tissue mass corrected bioscale of cerebral metabolic rate of oxygen consumption using 17-oxygen and 23-sodium MR imaging in a human brain at 9.4 T. Neuroimage 2010;51:723–733.
46. Ith M, Bigler P, Scheurer E, Kreis R, Hofmann L, Dirnhofer R, Boesch C. Observation and identification of metabolites emerging during postmortem decomposition of brain tissue by means of in situ 1H-magnetic resonance spectroscopy. Magn Reson Med 2002;48:915–920.
47. Fiat D, Ligeti L, Lyon RC, Ruttner Z, Pekar J, Moonen CTW, McLaughlin AC. In vivo 17O NMR study of rat brain during 17O2 inhalation. Magn Reson Med 1992;24:370–374.
48. Fiat D, Dolinsek J, Hankiewicz J, Dujovny M, Ausman J. Determination of regional cerebral oxygen consumption in the human: 17O natural abundance cerebral magnetic resonance imaging and spectroscopy in a whole body system. Neurol Res 1993;15:237–248.
49. Pekar J, Sinnwell T, Ligeti L, Chesnick AS, Frank JA, McLaughlin AC. Simultaneous measurement of cerebral oxygen consumption and blood flow using 17O and 19F magnetic resonance imaging. J Cereb Blood Flow Metab 1995;15:312–320.
50. Borowiak R, Groebner J, Haas M, Hennig J, Bock M. Direct cerebral and cardiac 17O-MRI at 3 Tesla: initial results at natural abundance. Magn Reson Mater Phy 2014;27:95–99.
51. Ernst RR, Anderson WA. Application of Fourier transform spectroscopy to magnetic resonance. Rev Sci Instrum 1966;37:93–102.